Chapter 1

Sensor-based Motion Control of Autonomous Underwater Vehicles, Part I: Modeling & Low Complexity State Estimation

George C. Karras[1] Charalampos P. Bechlioulis [1]Panos Marantos[1]Shahab Heshmati-alamdari[1]and Kostas J. Kyriakopoulos[1]

1.1 Introduction

In view of the increasingly demanding and complex missions envisioned for underwater robots, especially in the presence of environmental constraints, navigation and guidance systems with enhanced robustness need to be developed. Therefore, an accurate dynamic model of the underwater vehicle is essential in order to develop efficient control schemes. However, the complexity of the dynamic model may vary depending of the vehicle configuration, actuation capabilities, operating speed and planes of symmetry [1]. In that sense, the identification problem of underwater vehicles continues to pose considerable challenges to control system designers. Although the generic form of approximate lumped parameter finite-dimensional plant models for underwater vehicles is known [1], actual plant parameters (e.g., hydrodynamic added mass, buoyancy, and drag parameters) have to be determined.

Thus far, four commonly-used methods have been proposed to identify the dynamic model of underwater robotic vehicles. Captive model testing with a Planar Motion Mechanism (PMM) or other facilities is regarded as the most reliable one [2,3]. However, expensive infrastructure and very long and complex testings are required. On the other hand, estimation with empirical formulas is the most practical and convenient one [4], but provides reasonable results only for streamlined vehicles. Alternatively, numerical calculation based on Computational Fluid Dynamics (CFD) is a powerful modeling method [5], but its precision cannot be guaranteed a priori. Recently, System Identification (SI) approaches have become popular. Unlike the traditional naval architecture methods, this technique drastically reduces experimental time and is preferable because it makes use solely of the on-board sensors' data as well as of the excitation signals. Additionally, the technique is cost-effective

[1]School of Mechanical Engineering, Control Systems Lab, National Technical University of Athens, Greece {karrasg,chmpechl, marantos, shahab, kkyria}@mail.ntua.gr

and the repeatability is high. Thus, it is very suitable for underwater robotic vehicles of variable configuration, in which the payload and shape may change according to the mission.

Although most of the off-line techniques may provide sufficiently accurate results, they suffer from two major issues: i) in case the configuration of the vehicle changes the identification procedure should be repeated and ii) the evaluation of the estimated model follows the experimental procedure, thus poor identification results necessitate further experiments with different excitation signals. On the contrary, on-line identification is an on-the-fly process, where the estimation of the dynamic parameters occurs concurrently with the data acquisition process during the real-time operation of the system. Smallwood and Whitcomb in [6] as well as McFarland and Whitcomb in [7] describe an on-line adaptive technique with local stability proof for the identification of a finite dimensional dynamical model of dynamically positioned vehicles. Van de Ven et al. [8] and Ishii et al. [9] discuss the use of neural networks with on-line adaptation laws for identifying the dynamic model of underwater robotic vehicles. Eng et al. [10] propose an on-line system identification procedure based on a state variable filter and a recursive least square (SVF-RLS) estimator in order to determine the unknown dynamic parameters related to the yaw Degrees-of-Freedom (DoF) of a Unmanned Underwater Vehicle (UUV). Finally, an on-line identification scheme based on a global derivative-free optimization algorithm was presented in [11].

Efficient methods for on-line system identification have also been built based on the well-known Kalman filter [12]. More specifically, a Kalman filter with a maximum likelihood estimation approach was presented in [13]. A description of the Unscented Kalman Filter (UKF)'s applicability for the state and parameter estimation of non–linear systems, as well as an analytical justification of the superiority of the UKF over the Extended Kalman Filter (EKF) parameter estimation techniques have been provided by der Merwe and Wan in [14], and VanDyke et al. [15]. In the same direction, Karras et al. [16] described a dual UKF algorithm for on-line state and parameter estimation of underwater vehicles.

In this chapter, we describe the kinematic and dynamic equations of underwater robotic vehicles including standard assumptions and simplifications that may lead to low-complexity but accurate and operational models. Furthermore, we describe a Recursive Least Squares method for the on–line identification of the vehicle dynamic parameters. In addition, we present a state estimation technique, which according to the available sensors, can be adopted for either shallow or deep water operation. Keeping in mind low-complexity requirements, the proposed state estimation method is based on the Complementary Filters notion. The goal of this chapter is to provide the reader with the appropriate analytical methods, in order to derive a simple yet accurate vehicle model, design a state estimation algorithm that could be easily integrated into the embedded system framework of an underwater robotic vehicle and perform a fast on–line dynamic parameter identification.

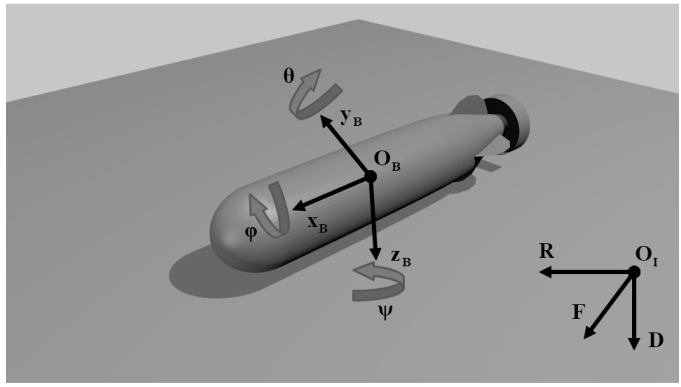

Figure 1.1: Underwater Vehicle Frames

1.2 Underwater Vehicle Kinematics & Dynamics

1.2.1 General Representation

Let us define a body-fixed frame $\boldsymbol{B} = \{e_x, e_y, e_z\}$ attached to the vehicle's center of gravity, as shown in 1.1, and an inertial frame $\boldsymbol{I} = \{e_F, e_R, e_D\}$ located at a fix position $O_{\boldsymbol{I}}$ within the workspace of the vehicle. Following standard modeling techniques [1], the dynamic model of the vehicle in the body fixed frame may be derived from the general Newton-Euler motion equations of a 6-DoF rigid body subject to external forces and torques in a fluid medium, as follows:

$$\begin{aligned} \boldsymbol{M}\dot{\boldsymbol{\nu}} + \boldsymbol{C}(\boldsymbol{\nu})\boldsymbol{\nu} + \boldsymbol{D}(\boldsymbol{\nu})\boldsymbol{\nu} + \boldsymbol{g}(\boldsymbol{\eta}) &= \boldsymbol{\tau}_E + \boldsymbol{\tau} \\ \dot{\boldsymbol{\eta}} &= \boldsymbol{J}(\boldsymbol{\eta})\boldsymbol{\nu} \end{aligned} \tag{1.1}$$

where:

- $\boldsymbol{\eta} \triangleq \left[\boldsymbol{\eta_1}^T \ \boldsymbol{\eta_2}^T\right]^T \in \mathbb{R}^6$ is the pose vector expressed in $\boldsymbol{I}$, that involves the position (i.e., $\boldsymbol{\eta_1} \triangleq [x\ y\ z]^T$) and orientation (i.e., $\boldsymbol{\eta_2} \triangleq [\phi\ \theta\ \psi]^T$) vectors;
- $\boldsymbol{\nu} \triangleq \left[\boldsymbol{\nu_1}^T \ \boldsymbol{\nu_2}^T\right]^T \in \mathbb{R}^6$ is the velocity vector expressed in $\boldsymbol{B}$, that involves the linear (i.e., $\boldsymbol{\nu_1} \triangleq [u\ v\ w]^T$) and angular (i.e., $\boldsymbol{\nu_2} \triangleq [p\ q\ r]^T$) velocity vectors;
- $\boldsymbol{\tau}_E \in \mathbb{R}^6$ is the total environmental force/torque vector expressed in $\boldsymbol{B}$, that is applied on the vehicle;
- $\boldsymbol{\tau} \triangleq [\tau_X,\ \tau_Y,\ \tau_Z,\ \tau_K,\ \tau_M,\ \tau_N]^T \in \mathbb{R}^6$ is the total propulsion vector (i.e., the body forces $\tau_X,\ \tau_Y,\ \tau_Z$ and torques $\tau_K,\ \tau_M,\ \tau_N$ generated by the actuators) applied on the vehicle and expressed in $\boldsymbol{B}$;
- $\boldsymbol{M} \triangleq \boldsymbol{M}_{RB} + \boldsymbol{M}_A$, where $\boldsymbol{M}_{RB} \in \mathbb{R}^{6\times6}$ and $\boldsymbol{M}_A \in \mathbb{R}^{6\times6}$ are the rigid body and added mass inertia matrices respectively;
- $\boldsymbol{C}(\boldsymbol{\nu}) \triangleq \boldsymbol{C}_{RB}(\boldsymbol{\nu}) + \boldsymbol{C}_A(\boldsymbol{\nu})$, where $\boldsymbol{C}_{RB}(\boldsymbol{\nu}) \in \mathbb{R}^{6\times6}$ and $\boldsymbol{C}_A(\boldsymbol{\nu}) \in \mathbb{R}^{6\times6}$ are the rigid body and added mass matrices that model the Coriolis and centrifugal effects respectively;
- $\boldsymbol{D}(\boldsymbol{\nu}) \triangleq \boldsymbol{D}_{quad}(\boldsymbol{\nu}) + \boldsymbol{D}_{lin}$, where $\boldsymbol{D}_{quad}(\boldsymbol{\nu}) \in \mathbb{R}^{6\times6}$ and $\boldsymbol{D}_{lin} \in \mathbb{R}^{6\times6}$ denote the quadratic and linear drag matrices respectively;

- $\boldsymbol{g}(\boldsymbol{\eta}) \in \mathbb{R}^6$ is the hydrostatic restoring force vector;
- $\boldsymbol{J}(\boldsymbol{\eta}) \triangleq \begin{bmatrix} \boldsymbol{J}_1(\boldsymbol{\eta_2}) & \mathbf{O}_3 \\ \mathbf{O}_3 & \boldsymbol{J}_2(\boldsymbol{\eta_2}) \end{bmatrix}$ is the Jacobian matrix transforming the velocities from the body-fixed frame $\boldsymbol{B}$ to the inertial frame $\boldsymbol{I}$, in which $\boldsymbol{J}_1(\boldsymbol{\eta_2}) \in SO(3)$ stands for the rotation matrix and $\boldsymbol{J}_2(\boldsymbol{\eta_2}) \in \mathbb{R}^{3\times 3}$ denotes the lumped transformation matrix;

Although (1.1) is highly non-linear, by applying proper algebraic manipulations, the dynamic model of the vehicle in the body fixed frame may be written in the following linear with respect to the dynamic parameters form:

$$\boldsymbol{\tau} = \boldsymbol{Y}(\boldsymbol{\eta}, \boldsymbol{\nu}, \dot{\boldsymbol{\nu}})\,\boldsymbol{\pi} \tag{1.2}$$

where the elements of the vector $\boldsymbol{\pi}$ involve the unknown parameters of: i) the inertia matrix $\boldsymbol{M}$, ii) the Coriolis and centrifugal matrix $\boldsymbol{C}(\boldsymbol{\nu})$, iii) the drag matrix $\boldsymbol{D}(\boldsymbol{\nu})$ and iv) the hydrostatic force vector $\boldsymbol{g}(\boldsymbol{\eta})$.

Remark 1: *The form appearing in* (1.2) *can be very practical for system identification procedures, since linear representation encourages the employment of Least Squares approximation methods, which are of low complexity and may deliver accurate results given a proper set of input-output measurements.*

The expanded form of the matrices appear in Eq.1.1, for a generic $6-DoF$ underwater vehicle, are given as follows [1]:

- $\boldsymbol{M_{RB}} = \begin{bmatrix} m & 0 & 0 & 0 & mz_G & -my_G \\ 0 & m & 0 & -mz_G & 0 & mx_G \\ 0 & 0 & m & my_G & -mx_G & 0 \\ 0 & -mz_G & my_G & I_x & -I_{xy} & -I_{xz} \\ mz_G & 0 & -mx_G & -I_{yx} & I_y & -I_{yz} \\ -my_G & mx_G & 0 & -I_{zx} & -I_{zy} & I_z \end{bmatrix}$

- $\boldsymbol{M_A} = -\begin{bmatrix} X_{\dot{u}} & X_{\dot{\upsilon}} & X_{\dot{w}} & X_{\dot{p}} & X_{\dot{q}} & X_{\dot{r}} \\ Y_{\dot{u}} & Y_{\dot{\upsilon}} & Y_{\dot{w}} & Y_{\dot{p}} & Y_{\dot{q}} & Y_{\dot{r}} \\ Z_{\dot{u}} & Z_{\dot{\upsilon}} & Z_{\dot{w}} & Z_{\dot{p}} & Z_{\dot{q}} & Z_{\dot{r}} \\ K_{\dot{u}} & K_{\dot{\upsilon}} & K_{\dot{w}} & K_{\dot{p}} & K_{\dot{q}} & K_{\dot{r}} \\ M_{\dot{u}} & M_{\dot{\upsilon}} & M_{\dot{w}} & M_{\dot{p}} & M_{\dot{q}} & M_{\dot{r}} \\ N_{\dot{u}} & N_{\dot{\upsilon}} & N_{\dot{w}} & N_{\dot{p}} & N_{\dot{q}} & N_{\dot{r}} \end{bmatrix}$

- $\boldsymbol{C_{RB}} = \begin{bmatrix} 0 & 0 & 0 & m(y_Gq+z_Gr) & -m(x_Gq-w) & -m(x_Gr+\upsilon) \\ 0 & 0 & 0 & -m(y_Gp+w) & m(z_Gr+x_Gp) & -m(y_Gr-u) \\ 0 & 0 & 0 & -m(z_Gp-\upsilon) & -m(z_Gq+u) & m(x_Gp+y_Gq) \\ -m(y_Gq+z_Gr) & m(y_Gp+w) & m(z_Gp-\upsilon) & 0 & -I_{yz}q-I_{xz}p+I_zr & I_{yz}r+I_{xy}p-I_yq \\ m(x_Gq-w) & -m(z_Gr+x_Gp) & m(z_Gq+u) & I_{yz}q+I_{xz}p-I_zr & 0 & -I_{xz}r-I_{xy}q+I_xp \\ m(x_Gr+\upsilon) & m(y_Gr-u) & -m(x_Gp+y_Gq) & -I_{yz}r-I_{xy}p+I_yq & I_{xz}r+I_{xy}q-I_xp & 0 \end{bmatrix}$

- $\boldsymbol{C_A(\nu)} = \begin{bmatrix} 0 & 0 & 0 & 0 & -\alpha_3 & \alpha_2 \\ 0 & 0 & 0 & \alpha_3 & 0 & -\alpha_1 \\ 0 & 0 & 0 & -\alpha_2 & \alpha_1 & 0 \\ 0 & -\alpha_3 & \alpha_2 & 0 & -b_3 & b_2 \\ \alpha_3 & 0 & -\alpha_1 & b_3 & 0 & -b_1 \\ -\alpha_2 & \alpha_1 & 0 & -b_2 & b_1 & 0 \end{bmatrix}$, where:

$$\begin{aligned}
\alpha_1 &= X_{\dot{u}}u + X_{\dot{\upsilon}}\upsilon + X_{\dot{w}}w + X_{\dot{p}}p + X_{\dot{q}}q + X_{\dot{r}}r \\
\alpha_2 &= X_{\dot{\upsilon}}u + Y_{\dot{\upsilon}}\upsilon + Y_{\dot{w}}w + Y_{\dot{p}}p + Y_{\dot{q}}q + Y_{\dot{r}}r \\
\alpha_3 &= X_{\dot{w}}u + Y_{\dot{w}}\upsilon + Z_{\dot{w}}w + Z_{\dot{p}}p + Z_{\dot{q}}q + Z_{\dot{r}}r \\
b_1 &= X_{\dot{p}}u + Y_{\dot{p}}\upsilon + Z_{\dot{p}}w + K_{\dot{p}}p + K_{\dot{q}}q + K_{\dot{r}}r \\
b_2 &= X_{\dot{q}}u + Y_{\dot{q}}\upsilon + Z_{\dot{q}}w + K_{\dot{q}}p + M_{\dot{q}}q + M_{\dot{r}}r \\
b_2 &= X_{\dot{r}}u + Y_{\dot{r}}\upsilon + Z_{\dot{r}}w + K_{\dot{r}}p + M_{\dot{r}}q + N_{\dot{r}}r
\end{aligned}$$

In most cases, the vehicle has three planes of symmetry, which further simplifies the representation of matrix $\boldsymbol{C_A(\nu)}$, according to [1]:

$$\boldsymbol{C_A(\nu)} = \begin{bmatrix} 0 & 0 & 0 & 0 & -Z_{\dot{w}}w & Y_{\dot{\upsilon}}\upsilon \\ 0 & 0 & 0 & Z_{\dot{w}}w & 0 & -X_{\dot{u}}u \\ 0 & 0 & 0 & -Y_{\dot{\upsilon}}\upsilon & X_{\dot{u}}u & 0 \\ 0 & -Z_{\dot{w}}w & Y_{\dot{\upsilon}}\upsilon & 0 & -N_{\dot{r}}r & M_{\dot{q}}q \\ Z_{\dot{w}}w & 0 & -X_{\dot{u}}u & N_{\dot{r}}r & 0 & -K_{\dot{p}}p \\ -Y_{\dot{\upsilon}}\upsilon & X_{\dot{u}}u & 0 & -M_{\dot{q}}q & K_{\dot{p}}p & 0 \end{bmatrix}$$

- $\boldsymbol{D}(\boldsymbol{\nu}) \triangleq \boldsymbol{D}_{lin} + \boldsymbol{D}_{quad}(\boldsymbol{\nu})$

$$\boldsymbol{D}_{lin} = -\begin{bmatrix} X_u & 0 & 0 & 0 & 0 & 0 \\ 0 & Y_\upsilon & 0 & 0 & 0 & 0 \\ 0 & 0 & Z_w & 0 & 0 & 0 \\ 0 & 0 & 0 & K_p & 0 & 0 \\ 0 & 0 & 0 & 0 & M_q & 0 \\ 0 & 0 & 0 & 0 & 0 & N_r \end{bmatrix}$$

$$\boldsymbol{D}_{quad}(\boldsymbol{\nu}) = -\begin{bmatrix} X_{u|u|}|u| & 0 & 0 & 0 & 0 & 0 \\ 0 & Y_{\upsilon|\upsilon|}|\upsilon| & 0 & 0 & 0 & 0 \\ 0 & 0 & Z_{w|w|}|w| & 0 & 0 & 0 \\ 0 & 0 & 0 & K_{p|p|}|p| & 0 & 0 \\ 0 & 0 & 0 & 0 & M_{q|q|}|q| & 0 \\ 0 & 0 & 0 & 0 & 0 & N_{r|r|}|r| \end{bmatrix}$$

- $\boldsymbol{g}(\boldsymbol{\eta}) = \begin{bmatrix} (mg-B)s\theta \\ -(mg-B)c\theta s\varphi \\ -(mg-B)c\theta c\varphi \\ -(y_GW - y_BB)c\theta c\varphi + (z_GW - z_BB)c\theta s\varphi \\ (z_GW - z_BB)s\theta + (x_GW - x_BB)c\theta c\varphi \\ -(x_GW - x_BB)c\theta s\varphi - (y_GW - y_BB)s\theta \end{bmatrix}$

- $\boldsymbol{J}_1(\boldsymbol{\eta}_2) = \begin{bmatrix} c\psi c\theta & -s\psi c\varphi + c\psi s\theta s\varphi & s\psi s\varphi + c\psi c\varphi s\theta \\ s\psi c\theta & c\psi c\varphi + s\varphi s\theta s\psi & -c\psi s\varphi + s\theta s\psi c\varphi \\ -s\theta & c\theta s\varphi & c\theta c\varphi \end{bmatrix}$

- $\boldsymbol{J}_2(\boldsymbol{\eta}_2) = \begin{bmatrix} 1 & s\varphi t\theta & c\varphi t\theta \\ 0 & c\varphi & -s\varphi \\ 0 & s\varphi/c\theta & c\varphi/c\theta \end{bmatrix}$

where:

- m is the mass, g the gravity and B the buoyancy of the vehicle.
- x_G, y_G, z_G the position of the mass center with respect to the body frame $\boldsymbol{B}$.
- $(x)_{\dot{u}}$, $(x)_{\dot{v}}$, $(x)_{\dot{w}}$, $(x)_{\dot{p}}$, $(x)_{\dot{q}}$, $(x)_{\dot{r}}$, for $x \in \{X,Y,Z,K,M,N\}$ the added mass terms according to [1].
- I_x, I_y, I_z, I_{xy},I_{yx},I_{xz}, I_{zx}, I_{yz}, I_{zy} the moments of inertia along the respective axes
- X_u, $X_{|u|u}$, Y_v, $Y_{|v|v}$, Z_w, $Z_{|w|w}$, N_r, $N_{|r|r}$ are the 1^{st} and 2^{nd} order drag parameters according to [1].
- $s\cdot = \sin(\cdot)$, $c\cdot = \cos(\cdot)$, $t\cdot = \tan(\cdot)$

Consider a $6-DoF$ actuated vehicle with $i = 1...N$ thrusters. Each thruster produces the following vector of forces and torques with respect to the body fixed frame $\boldsymbol{B}$:

$$ {}^i\boldsymbol{\tau} = \begin{bmatrix} {}^iT \\ {}^iQ \end{bmatrix} = \begin{bmatrix} {}^iT\,{}^ie \\ {}^iT\left({}^iL \times {}^ie\right) \end{bmatrix} = \begin{bmatrix} {}^ie_x \\ {}^ie_y \\ {}^ie_z \\ \left({}^iL \times {}^ie\right)_x \\ \left({}^iL \times {}^ie\right)_y \\ \left({}^iL \times {}^ie\right)_z \end{bmatrix} {}^iT \tag{1.3} $$

where ${}^ie = \begin{bmatrix} {}^ie_x & {}^ie_y & {}^ie_z \end{bmatrix}^T = \begin{bmatrix} \cos\psi_T^i \cos\theta_T^i \\ \sin\psi_T^i \cos\theta_T^i \\ -\sin\theta_T^i \end{bmatrix}$ is the orientation of the thruster i relatively to the body fixed frame $\boldsymbol{B}$ and ${}^iL = \begin{bmatrix} l_i^x & l_i^y & l_i^z \end{bmatrix}^T$ determines the position of the point of attack for ${}^iT$ relatively to $\boldsymbol{B}$. Superposition of the individual contributions ${}^i\boldsymbol{\tau}$ leads to total vector of propulsion forces and torques:

$$ \boldsymbol{\tau} = \begin{bmatrix} X \\ Y \\ Z \\ K \\ M \\ N \end{bmatrix} = \sum_i^N {}^i\tau = \sum_i^N \begin{bmatrix} {}^ie \\ \left({}^iL \times {}^ie\right) \end{bmatrix} {}^iT = \begin{bmatrix} {}^1e_x & {}^ie_x & {}^Ne_x \\ {}^1e_y & {}^ie_y & {}^Ne_y \\ {}^1e_z & {}^ie_z & {}^Ne_z \\ \left({}^1L \times {}^1e\right)_x & \cdots \left({}^iL \times {}^ie\right)_x \cdots & \left({}^NL \times {}^Ne\right)_x \\ \left({}^1L \times {}^1e\right)_y & \left({}^iL \times {}^ie\right)_y & \left({}^NL \times {}^Ne\right)_y \\ \left({}^1L \times {}^1e\right)_z & \left({}^iL \times {}^ie\right)_z & \left({}^NL \times {}^Ne\right)_z \end{bmatrix} \begin{bmatrix} {}^1T \\ \cdot \\ \cdot \\ \cdot \\ {}^iT \\ \cdot \\ \cdot \\ \cdot \\ {}^NT \end{bmatrix} \tag{1.4} $$

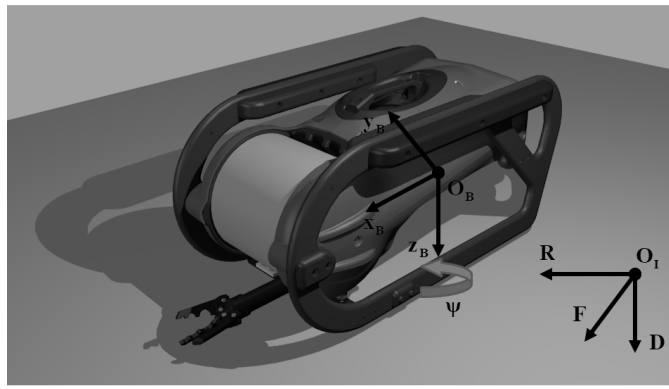

Figure 1.2: Seabotix LBV Frames

1.2.2 Modeling and On–line Parameter Identification Example: 4 DoFs Underwater Vehicle

In this section, we provide a modeling and on–line parameter identification example of a 4 DoFs underwater robotic vehicle, Seabotix LBV150 [17], as shown in Fig. 1.2, actuated in Surge, Sway, Heave, and Yaw via a four thruster set configuration. We begin from the general 6 DoF representation and according to particular assumptions and simplifications that apply to the specific vehicle, we derive the dynamic and kinematic equations describing its motion. Then, we reformulate the system into a linear with respect to its dynamic parameters form and employ a conventional constrained Recursive-Least-Squares (RLS) method [18]. For the vehicle under investigation, the following properties hold:

- the gravity center and the origin of body frame $\boldsymbol{B}$ coincide, thus $x_G = y_G = z_G = 0$
- the buoyancy and gravity center coincide, thus $x_B = y_B = z_B = 0$
- the vehicle mass is symmetric in all axis, thus M_A has elements only in the main diagonal and $I_{xy} = I_{xz} = I_{yx} = I_{yz} = I_{zx} = I_{zy} = 0$
- the vehicle is under-actuated about Roll and Pitch axes. Thus, the 4th and 5th rows and columns of $\boldsymbol{M_{RB}}, \boldsymbol{M_A}, \boldsymbol{C_{RB}}, \boldsymbol{C_A(\nu)}, \boldsymbol{D(\nu)}$, and 4th and 5th row of $\boldsymbol{g(\eta)}$ are omitted.

Considering the above properties, the 4 DoF vehicle equations of motion are given in analytical form as follows :

$$\begin{aligned}
&\dot{u}(m+X_{\dot{u}}) - vr(m+Y_{\dot{v}}) + qw(m+Z_{\dot{w}}) - uX_u - u|u|X_{u|u|} - \sin\theta\,(mg-B) = \tau_x \\
&\dot{v}(m+Y_{\dot{v}}) + ur(m+X_{\dot{u}}) - pw(m+Z_{\dot{w}}) - vY_v - v|v|Y_{v|v|} + \sin\varphi\cos\theta\,(mg-B) = \tau_y \\
&\dot{w}(m+Z_{\dot{w}}) - uq(m+X_{\dot{u}}) + uv(m+Y_{\dot{v}}) - wZ_w - w|w|Z_{w|w|} + \cos\varphi\cos\theta\,(mg-B) = \tau_z \\
&\dot{r}(I_z+N_{\dot{r}}) - uv(m+X_{\dot{u}}) + uv(m+Y_{\dot{v}}) - rN_r - r|r|N_{r|r|} = \tau_N
\end{aligned} \tag{1.5}$$

In terms of actuation, the Seabotix LBV150 is equipped with 4 thrusters, i.e., Port (p), Starboard (s), Vertical (v), Lateral (l), which are effective in Surge (X),

Sway (Y), Heave (Z) and Yaw (N) motion, as shown in Fig. **??**. Hence, the generalized force/torque input vector $\boldsymbol{\tau}$ is given by:

$$\boldsymbol{\tau} = \begin{bmatrix} X \\ Y \\ Z \\ K \\ M \\ N \end{bmatrix} = \begin{bmatrix} {}^{p}e_x & {}^{s}e_x & {}^{v}e_x & {}^{l}e_x \\ {}^{p}e_y & {}^{s}e_y & {}^{v}e_y & {}^{l}e_y \\ {}^{p}e_z & {}^{s}e_z & {}^{v}e_z & {}^{l}e_z \\ ({}^{p}L \times {}^{p}e)_x & ({}^{s}L \times {}^{s}e)_x & ({}^{v}L \times {}^{v}e)_x & ({}^{l}L \times {}^{l}e)_x \\ ({}^{p}L \times {}^{p}e)_y & ({}^{s}L \times {}^{s}e)_y & ({}^{v}L \times {}^{v}e)_y & ({}^{l}L \times {}^{l}e)_y \\ ({}^{p}L \times {}^{p}e)_z & ({}^{s}L \times {}^{s}e)_z & ({}^{v}L \times {}^{v}e)_z & ({}^{l}L \times {}^{l}e)_z \end{bmatrix} \begin{bmatrix} \tau_p \\ \tau_s \\ \tau_v \\ \tau_l \end{bmatrix} \quad (1.6)$$

where $X = \tau_X, Y = \tau_Y, Z = \tau_Z, N = \tau_N$.

By substituting in (1.6) the actual position and orientation of each thruster with respect to body frame $\boldsymbol{B}$, we derive the thruster allocation matrix $\boldsymbol{T}_{\mathbb{A}}$for Seabotix LBV150:

- ${}^{p}L = \begin{bmatrix} -0.135 & -0.0475 & 0 \end{bmatrix}^T, {}^{s}L = \begin{bmatrix} -0.135 & 0.0475 & 0 \end{bmatrix}^T, {}^{v}L = \begin{bmatrix} 0 & 0 & -0.05 \end{bmatrix}^T$, ${}^{l}L = \begin{bmatrix} 0.05 & 0.05 & 0 \end{bmatrix}^T$
- ${}^{p}e = \begin{bmatrix} 1 & 0 & 0 \end{bmatrix}^T, {}^{s}e = \begin{bmatrix} 1 & 0 & 0 \end{bmatrix}^T, {}^{l}e = \begin{bmatrix} 0 & 1 & 0 \end{bmatrix}^T, {}^{v}e = \begin{bmatrix} 0 & 0 & 1 \end{bmatrix}^T$

$$\boldsymbol{T}_{\mathbb{A}} = \begin{bmatrix} 1 & 1 & 0 & 0 \\ 0 & 0 & 1 & 0 \\ 0 & 0 & 0 & 1 \\ 0 & 0 & 0 & 0 \\ 0 & 0 & 0 & 0 \\ 0.0475 & -0.0475 & 0.05 & 0 \end{bmatrix} \quad (1.7)$$

By employing the appropriate algebraic manipulation we can reformulate (1.5) to a linearly independent with respect to the dynamic parameters form (1.2), as follows:

$$\overbrace{\begin{bmatrix} \tau_X \\ \tau_Y \\ \tau_Z \\ \tau_N \end{bmatrix}}^{\boldsymbol{\tau}_{4d}} = \overbrace{\begin{bmatrix} \hat{u} & -\hat{v}r & q\hat{w} & 0 & -\hat{u} & -\hat{u}|\hat{u}| & 0 & 0 & 0 & 0 & 0 & 0 & -\mathbf{s}_\theta \\ \hat{u}r & \hat{v} & -p\hat{w} & 0 & 0 & 0 & -\hat{v} & -\hat{v}|\hat{v}| & 0 & 0 & 0 & 0 & \mathbf{s}_\phi \mathbf{c}_\theta \\ -\hat{u}q & \hat{v}p & \hat{w} & 0 & 0 & 0 & 0 & 0 & -\hat{w} & -\hat{w}|\hat{w}| & 0 & 0 & \mathbf{c}_\phi \mathbf{c}_\theta \\ -\hat{u}\hat{v} & \hat{u}\hat{v} & 0 & \dot{r} & 0 & 0 & 0 & 0 & 0 & 0 & -r & -r|r| & 0 \end{bmatrix}}^{\mathbf{Y}_{4d}} \overbrace{\begin{bmatrix} \hat{\boldsymbol{\pi}}_{\mathbf{MC}} \\ \hat{\boldsymbol{\pi}}_{\mathbf{D}} \\ \hat{\pi}_{\boldsymbol{g}} \end{bmatrix}}^{\hat{\boldsymbol{\pi}}} \quad (1.8)$$

where $\boldsymbol{\tau}_{4d}$ stands for the overall actuation of the system and $\hat{\boldsymbol{\pi}}$ represents the estimate of the unknown parameters $\pi = [\pi_{\mathbf{MC}}^T, \pi_{\mathbf{D}}^T, \pi_{\boldsymbol{g}}^T]^T$ with:

$$\pi_{\mathbf{MC}} = \begin{bmatrix} m + X_{\dot{u}},\ m + Y_{\dot{v}},\ m + Z_{\dot{w}}\ I_z + N_{\dot{r}} \end{bmatrix}^T \in \mathbb{R}^4 \quad (1.9)$$

$$\pi_{\mathbf{D}} = \begin{bmatrix} X_u,\ X_{|u|u},\ Y_v,\ Y_{|v|v},\ Z_w,\ Z_{|w|w},\ N_r,\ N_{|r|r} \end{bmatrix}^T \in \mathbb{R}^8 \quad (1.10)$$

$$\pi_{\boldsymbol{g}} = mg - B \quad (1.11)$$

denoting the unknown (added) masses and (added) inertia (1.9), the unknown 1^{st} and 2^{nd} order drag parameters (1.10) and the difference of gravity mg and buoyancy B (1.11) respectively [1]. An analytical description of the dynamic parameters is given below:

- m is the mass of the vehicle
- $X_{\dot{u}}, Y_{\dot{v}}, Z_{\dot{w}}, N_{\dot{r}}$ are the added masses along Surge, Sway, Heave and Yaw respectively. Added mass should be understood as pressure-induced forces and moments due to a forced harmonic motion of the body which are proportional to the acceleration of the body. Consequently, the added mass forces and the acceleration will be 180 degrees out of phase to the forced harmonic motion [1]. More specific it stands: $X_{\dot{u}} \triangleq \frac{\partial X}{\partial \dot{u}}$, $Y_{\dot{v}} \triangleq \frac{\partial Y}{\partial \dot{v}}$, $Z_{\dot{w}} \triangleq \frac{\partial Z}{\partial \dot{w}}$, $N_{\dot{r}} \triangleq \frac{\partial N}{\partial \dot{r}}$.
- X_u, Y_v, Z_w, N_r are the linear and $X_{|u|u}$, $Y_{|v|v}$, $Z_{|w|w}$, $N_{|r|r}$ the quadratic damping terms along Surge, Sway, Heave and Yaw respectively. In general, the damping of an underwater vehicle will be highly nonlinear and coupled. Nevertheless, one rough approximation could be to assume that the vehicle is performing a non-coupled motion, has three planes of symmetry and that terms higher than second order are negligible. This suggests a diagonal structure of the total hydrodynamic damping matrix $D(v)$ with only linear and quadratic damping terms on the diagonal.
- g is the gravity.
- B is the buoyancy.

Even though the equations of motion are non-linear, the vehicle is input to state stable. Therefore, bounded inputs will never exhibit instability. This comes from the hydrodynamic terms and the neutral buoyancy properties which make the vehicle passive by construction. For that reason we are allow to employ open loop sinusoidal and step inputs for the excitation of the system.

Following [18], the constraint RLS algorithm is formulated as:

$$\mathbf{K}_k = \mathbf{P}_{k-1}\mathbf{Y}_{4d,k-1}^T \left(\mathbf{Y}_{4d,k-1}\mathbf{P}_{k-1}\mathbf{Y}_{4d,k-1}^T + \mathbf{R}_\tau\right)^{-1} \tag{1.12}$$

$$\mathbf{P}_k = \mathbf{P}_{k-1} - \mathbf{K}_k\mathbf{Y}_{4d,k-1}^T\mathbf{P}_{k-1} \tag{1.13}$$

$$\hat{\boldsymbol{\pi}}_k = \mathbf{Proj}\left\{\hat{\boldsymbol{\pi}}_{k-1} + \mathbf{K}_k\left(\boldsymbol{\tau}_{4d,k-1} - \mathbf{Y}_{4d,k-1}^T\hat{\boldsymbol{\pi}}_{k-1}\right)\right\} \tag{1.14}$$

where $\mathbf{P} \in \mathbb{R}^{13\times13}$ denotes the weighted sample covariance matrix, $\mathbf{R}_\tau \in \mathbb{R}^{4\times4}$ is a constant diagonal matrix of the noise of the system and the projection operator $\mathbf{Proj}\{\cdot\}$ is adopted to enforce $\hat{\boldsymbol{\pi}}_{\mathbf{MC}} > 0$, $\hat{\boldsymbol{\pi}}_{\mathbf{D}} < 0$ and $\hat{\pi}_{\boldsymbol{g}} < 0$.

It is well-recognized that reliable, accurate and efficient system identification requires appropriately designed experiments. When designing an identification experiment, it is essential to ensure that the excitation is sufficient to provide accurate and fast parameter estimation in the presence of measurement noise and actuator disturbances. In our approach, the excitation module is in charge of delivering the appropriate inputs (i.e., excitation trajectories) in the form of body forces and torques during the identification procedure. We propose a decision making algorithm (see Fig. 1.3), which employs four different excitation modes depending on the DoF that is currently under investigation, as well as an extra mode, where the vehicle is excited along all actuated DoFs simultaneously. Thus, we identify the following modes of excitation: *1) modeYaw, 2) modeSurge, 3) modeSway, 4) modeHeave, 5) modeTotal*. In modes *1-4*, the vehicle is actuated only along the corresponding DoF, whereas in *modeTotal* all actuated DoFs are simultaneously excited. The transition from a mode of excitation to its subsequent is decided by monitoring the convergence of

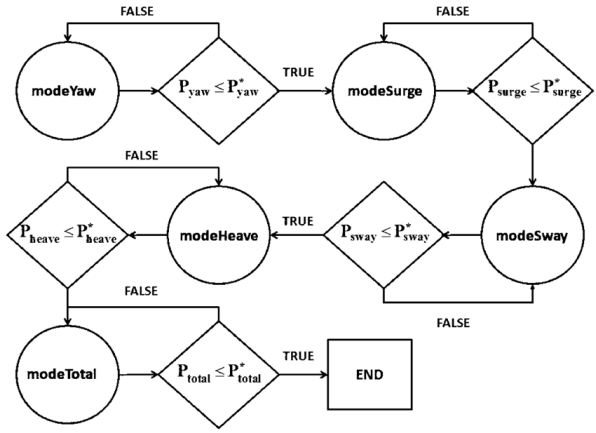

Figure 1.3: The decision making algorithm of the proposed Excitation Module.

the dynamic parameters that are related to the individual DoF. More specifically, the convergence metric is evaluated by adding the appropriate diagonal elements of the covariance matrix $\mathbf{P}_k$ defined in (1.13), as follows:

$$\begin{aligned}
P^k_{surge} &= P^k_{m+X_{\dot{u}}} + P^k_{X_u} + P^k_{X_{u|u|}} \\
P^k_{sway} &= P^k_{m+Y_{\dot{v}}} + P^k_{Y_v} + P^k_{Y_{v|v|}} \\
P^k_{heave} &= P^k_{m+Z_{\dot{w}}} + P^k_{Z_w} + P^k_{Z_{w|w|}} + P^k_{mg-B} \\
P^k_{yaw} &= P^k_{m+N_{\dot{r}}} + P^k_{N_r} + P^k_{N_{r|r|}} \\
P^k_{total} &= trace(P_k)
\end{aligned} \tag{1.15}$$

where P^k_{surge}, P^k_{sway}, P^k_{heave}, P^k_{yaw}, P^k_{total} are the estimates of the covariances related to Surge, Sway, Heave and Yaw DoFs respectively. The term P^k_{total} is the trace of the overall covariance matrix P^k and it is used for the final assessment of the identified dynamic model via concurrent excitation along all actuated DoFs. In order to proceed to the next excitation mode, the metric P^k_i, $i \in \{surge, sway, heave, yaw, total\}$ which is calculated during the on-line identification should become smaller than a default threshold value $P^\star_i$, $i \in \{surge, sway, heave, yaw, total\}$ as depicted in Fig. 1.3.

Each of the aforementioned excitation modes employs an internal functionality, which comprises of three distinct submodules, namely *subMode0, subMode1, subMode2*. In particular, *subMode0* provides periodical inputs to the system with random amplitudes and frequencies in order to identify the parameters related to the (added) inertia, (added) mass and gravity/buoyancy terms of the vehicle. After a finite predefined time frame, *subMode1* is engaged, which in turn provides step inputs with random and relatively small amplitudes, in order to identify the

Algorithm 1 The Internal mode functionality

$SMcounter \leftarrow SMcounter + 1$ ▷ Increment sub mode counter (e.g. subMode0) by 1
if $SMcounter \geq SMcounterMax$ **then** ▷ Check if mode counter has exceed the maximum number of iterations
  $submode \leftarrow (submode + 1)\%3$ ▷ If so progress to next mode (e.g from subMode0 to subMode1)
  $SMcounter \leftarrow 0$ ▷ Set sub mode counter to zero
  $INTcounter \leftarrow INTcounterMax$
end if
if $submode = 0$ `True` **then** ▷ Check if subMode0 is enabled
  if $INTcounter \geq INTcounterMax$ **then**
    $f \leftarrow rand(0, f_{max})$ ▷ Calculate a random frequency between (0, fmax)
    $a \leftarrow \tau_{max}$ ▷ Assign a maximum amplitude value
    $\tau \leftarrow a \cdot \cos(f \cdot t)$ ▷ Calculate sinusoidal input
    $INTcounter \leftarrow 0$
  end if
  $INTcounter \leftarrow INTcounter + 1$
end if
if $submode = 1$ `True` **then** ▷ Check if subMode1 is enabled
  if $INTcounter \geq INTcounterMax$ **then**
    $\tau \leftarrow rand(0, \tau_{max}^{low}) \cdot rand(sign)$ ▷ Calculate random step signal (low speeds) either positive or negative
    $INTcounter \leftarrow 0$
  end if
  $INTcounter \leftarrow INTcounter + 1$
end if
if $submode = 2$ `True` **then** ▷ Check if subMode2 is enabled
  if $INTcounter \geq INTcounterMax$ **then**
    $\tau \leftarrow rand(\tau_{max}^{low}, \tau_{max}^{high}) \cdot rand(sign)$ ▷ Calculate random step signal (high speeds) either positive or negative
    $INTcounter \leftarrow 0$
  end if
  $INTcounter \leftarrow INTcounter + 1$

end if

first order hydrodynamic coefficients. Finally, *subMode2* is used to provide inputs for the identification of the second order hydrodynamic coefficients, via step inputs with random but larger amplitudes. An algorithmic representation of the aforementioned internal functionality is described in Algorithm 1. The procedure iterates infinitely until the higher level module reaches its performance goal $P_i^\star$, $i \in \{surge, sway, heave, yaw, total\}$ and proceeds to the subsequent mode of excitation as decided by the decision making algorithm presented previously.

1.3 State Estimation for Underwater Vehicles

The design of a state estimation module, is highly affected by the available navigation sensors and the vehicle model (kinematic and/or dynamic). It is well known that GPS sensors cannot operate properly in the underwater environment. Hence, acoustic, inertial and vision-based sensors are usually fused together to provide an accurate state estimation of the underwater vehicle. However, acoustic sensors such as Ultra Short Baseline (USBL) and Doppler Velocity Log (DVL) sensors, exhibit poor performance in shallow waters and constrained workspaces due to scattering effects. On the other hand, vision sensors may perform poorly in low visibility conditions which often occur in deep water operations. Thus, in most cases different sensor suites are employed for shallow and deep water missions. In the rest of this chapter, we present state estimation techniques based on the Complementary Filters notion for both shallow and deep water operations. In both cases we assume that the vehicle is equipped with an Attitude and Heading Reference System (AHRS), which successfully delivers 3D orientation, angular velocities and accelerations with respect to the vehicle body frame. Additionally, we assume that a depth sensor is also installed on the underwater vehicle. The aforementioned suite is quite standard

in almost all commercial and non-commercial underwater vehicles. The nature of the operating environment (i.e shallow or deep waters) highly affects the choice of additional navigation sensors.

1.3.1 Introduction to Complementary Filters

Complementary filters provide a solution of fusing two or more different sensors that measure the same quantity or its rate. The solution exploits the fact that the various sensors or models exhibit better behavior and performance in different bands of frequency. For example, for a simple integrator system (i.e., $\dot{x} = u$) and two sensors that measure x and u with measurement models defined as $z_x = x + n_x$ and $z_u = u + n_u + b(t)$, where $n_{x,u}$ are the measurements noise terms and b is a bias term that affects the z_u at low frequencies, the complementary filter can be written in frequency domain as $\hat{x} = L(s)z_x + H(s)\frac{z_u}{s}$, where $L(s)$ is a low-pass filter and $H(s)$ a high-pass filter that follow the equation $L(s) + H(s) = 1$, which is the main property of the complementary filters. Additionally, the selection of the order of $L(s)$ and $H(s)$ determines the order of the filter, respectively. In the majority of use cases, first-order filters are used by selecting: $L(s) = \frac{1}{1+T_c s}$ and $H(s) = \frac{T_c s}{1+T_c s}$, where $T_c = \frac{2\pi}{\omega_c}$ is the selected cut-off frequency for both filters. Using this estimator, the rate sensor z_u is firstly integrated to get the value of x. This could give unreliable results due to the bias term integration. For that reason, second-order filters are used by selecting: $L(s) = \frac{2\zeta\omega_c s+\omega_c^2}{s^2+2\zeta\omega_c s+\omega_c^2}$ and $H(s) = \frac{s^2}{s^2+2\zeta\omega_c s+\omega_c^2}$, where ζ is the damping factor of the filter. In practice, the discrete form of the complementary filters is used. Thus, the first order filter is written as:

$$\hat{x}_k = \hat{x}_k^- + k\left(z_x^k - \hat{x}_k^-\right) \tag{1.16}$$

where $\hat{x}_k^- = \hat{x}_{k-1} + \Delta t z_u^{k-1}$ is the a priori estimation of $\hat{x}$ and $k = \frac{\Delta t}{\Delta t + T_c}$ is the selected gain, while the second-order filters are written as:

$$\hat{x}_k = \hat{x}_k^- + k_p\left(z_x^k - \hat{x}_k^-\right),\ \hat{b}_k = \hat{b}_{k-1} - k_i\left(z_x^k - \hat{x}_k^-\right) \tag{1.17}$$

where the a priori estimation has been fixed by the bias term (i.e $\hat{x}_k^- = \hat{x}_{k-1} + \Delta t z_u^{k-1} - \Delta t\hat{b}_{k-1}$) and $k_p = \frac{\left(2\zeta\omega_c + \Delta t\omega_c^2\right)\Delta t}{1+\left(2\zeta\omega_c+\Delta t\omega_c^2\right)\Delta t}$, $k_i = \Delta t\,\omega_c^2\,(1-k_p)$ are the selected gains. Simple block diagrams that accompany the aforementioned discussion are illustrated in Fig. 1.4 and Fig. 1.5.

1.3.2 Complementary Filter Design

1.3.2.1 Shallow Waters Operation

In shallow waters, acoustic sensors such as DVL and USBL may perform poorly. A fairly accurate and low cost solution is the installation of a down-looking camera accompanied by a rigidly attached laser pointer which projects a dot inside the camera's field of view. The proposed setup is depicted in Fig. 1.6. Assuming fair

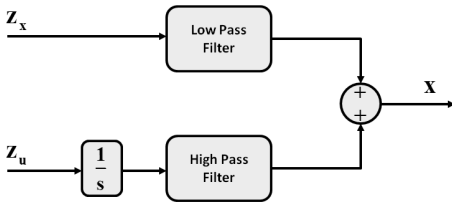

Figure 1.4: Simple First-order CF block diagram.

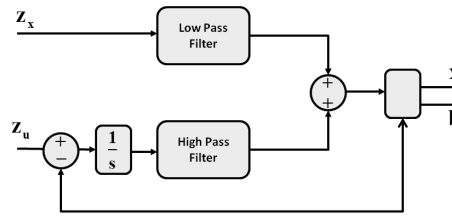

Figure 1.5: Simple Second-order CF block diagram.

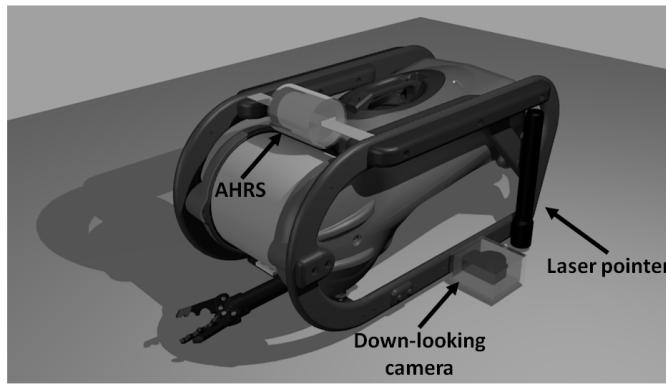

Figure 1.6: Sensor setup for shallow waters operation.

visibility and lighting conditions, the proposed laser-vision system is able to provide 3D translational velocities with respect to the vehicle body frame $\boldsymbol{B}$, via computer vision optical flow techniques, as well as pose estimation of the vehicle in case specific visual landmarks are located within the operating workspace. Next, we present the design of a complete state estimation algorithm, based on the Complementary Filters notion, assuming the vehicle is equipped with a down-looking camera, a laser pointer and an AHRS, in a landmark based environment. Following the concept of Complementary Filters as in [19], we propose a sensor fusion methodology that estimates the translational kinematics of the underwater vehicle (i.e., the position $\boldsymbol{\eta_1}$, the linear velocity $\boldsymbol{\nu_1}$ and the linear acceleration $\dot{\boldsymbol{\nu}}_{\boldsymbol{1}}$). We should note that the AHRS is assumed to deliver accurate and reliable 3D angles and angular velocities, due to the on-board– usually EKF based–navigation filter. Thus, AHRS measurements are considered as inputs to the system. The overall architecture of the proposed state estimation module is depicted in Fig. 1.7, while a detailed analysis follows below:

Owing to the high sampling frequency of the AHRS compared to the slow motion of the underwater vehicle, the translational kinematics can be written in discrete form as follows:

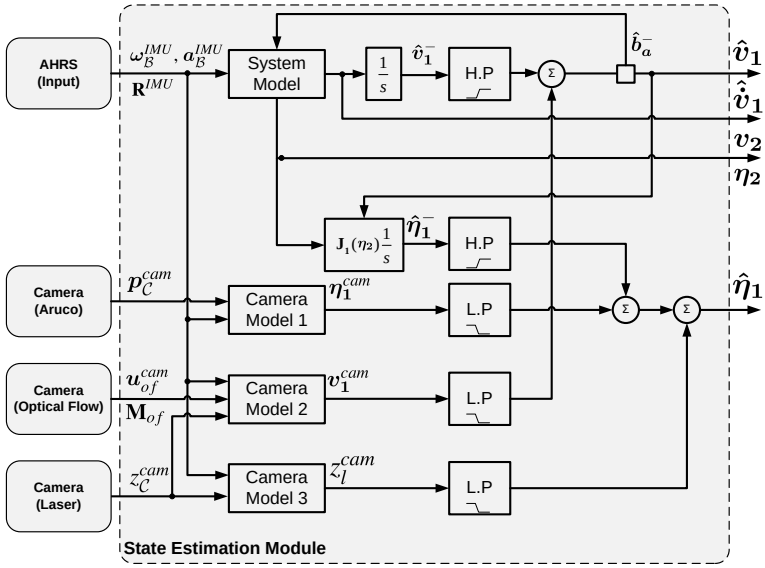

Figure 1.7: The proposed State Estimation Module for Shallow Waters.

$$\boldsymbol{\eta}_1^{k+1} = \boldsymbol{\eta}_1^k + \Delta t \mathbf{J}_1\left(\boldsymbol{n}_2^k\right)\boldsymbol{\nu}_1^k \tag{1.18}$$

$$\boldsymbol{\nu}_1^{k+1} = \boldsymbol{\nu}_1^k + \Delta t \boldsymbol{a}_{\mathcal{B}}^k \tag{1.19}$$

where $\boldsymbol{a}_{\boldsymbol{B}}^{\boldsymbol{k}} \in \mathbb{R}^3$ is the acceleration of the vehicle expressed in $\boldsymbol{B}$ and Δt denotes the time step of integration. The measurement model for each sensor is defined as follows:

- The AHRS of the vehicle consists of a 9-DoF Inertial Measurement Unit (IMU) that delivers the angular velocity measurement $\boldsymbol{\omega}_{\boldsymbol{B}}^{IMU}$, the acceleration measurement $\boldsymbol{a}_{\boldsymbol{B}}^{IMU}$ and the orientation of the vehicle expressed as a rotation matrix $\mathbf{R}^{IMU} \in SO(3)$. Thus:

$$\boldsymbol{\omega}_{\boldsymbol{B}}^{IMU} = \boldsymbol{\nu}_2 + \boldsymbol{w}_{\boldsymbol{\omega}} \tag{1.20}$$

$$\boldsymbol{a}_{\boldsymbol{B}}^{IMU} = \boldsymbol{a}_{\boldsymbol{B}} + \boldsymbol{b}_{\boldsymbol{a}} + \mathbf{R}^{IMU}\boldsymbol{g}_{\boldsymbol{N}} + \boldsymbol{w}_{\boldsymbol{a}} \tag{1.21}$$

$$\mathbf{R}^{IMU} = \mathbf{R}_{\boldsymbol{IN}}^T \mathbf{J}_1(\boldsymbol{\eta}_2) \tag{1.22}$$

$$\tag{1.23}$$

where $\boldsymbol{w}_{\boldsymbol{\omega}}$ and $\boldsymbol{w}_{\boldsymbol{a}}$ denote the guassian noises of the gyroscope and accelerometer sensors respectively, $\boldsymbol{b}_{\boldsymbol{a}} \in \mathbb{R}^3$ is the accelerometer bias, $\boldsymbol{g}_{\boldsymbol{N}} = [0\ 0\ g]^T$ denotes the gravity acceleration vector in the North-East-Down (NED) frame $\boldsymbol{N}$ and $\mathbf{R}_{\boldsymbol{IN}} \in SO(3)$ is a constant rotation matrix transforming any vector from the NED frame to the inertial frame $\boldsymbol{I}$.

Figure 1.8: The vision techniques applied for depth estimation, linear velocity estimation and localization.

- The camera is assumed to be fixed on the vehicle with no extra dynamics included and looking downwards. Thus, we define the frame $\mathcal{C} = \{e_{cx}, e_{cy}, e_{cz}\}$ attached at the center of the camera with a fixed orientation $\mathbf{R}_{\mathcal{C}}$ and translation $\boldsymbol{l}_{\mathcal{C}}$ with respect to $\boldsymbol{B}$. Employing three basic computer vision tools, i.e., a visual landmark based localization algorithm, the optical flow technique and a laser detection system [19–21] (see Fig. 1.8), we obtain the following essential state estimates: a) the vehicle position vector expressed in $\boldsymbol{I}$, b) the vehicle linear velocity expressed in $\boldsymbol{B}$ and c) the range between the vehicle and the sea bottom respectively. Hence, the camera measurement models can be defined as follows:

$$\boldsymbol{p}_{\mathcal{C}}^{cam} = \mathbf{R}_{\mathcal{C}} \left(\mathbf{J}_1^T \left(\boldsymbol{\eta}_{\mathbf{2}} \right) \boldsymbol{\eta}_{\mathbf{1}} + \boldsymbol{l}_{\mathcal{C}} \right) + \boldsymbol{w}_{\boldsymbol{p}}^{cam} \tag{1.24}$$

$$\boldsymbol{v}_{of}^{cam} = \frac{1}{z_{\mathcal{C}}^{cam}} \mathbf{R}_{\mathcal{C}} \left(\boldsymbol{v}_{\mathbf{1}} + \boldsymbol{v}_{\mathbf{2}} \times \boldsymbol{l}_{\mathcal{C}} \right) + \mathbf{M}_{of} \mathbf{R}_{\mathcal{C}} \boldsymbol{v}_{\mathbf{2}} + \boldsymbol{w}_{of}^{cam} \tag{1.25}$$

$$z_{\mathcal{C}}^{cam} = -\frac{z + \boldsymbol{l}_{\mathcal{C},3}}{J_{3,3}} + n_z^{cam} \tag{1.26}$$

  where $\boldsymbol{p}_{\mathcal{C}}^{cam}$ is the position measurement obtained from the landmark localization algorithm, that denotes the position of the camera with respect to $\boldsymbol{I}$ expressed in $\mathcal{C}$, $\boldsymbol{v}_{of}^{cam}$ denotes the optical flow velocity with gyro compensation from the optical flow data $\mathbf{M}_{of}$ and $z_{\mathcal{C}}^{cam}$ is the range between the camera and the sea bottom measured by the laser detection technique. Moreover, $\boldsymbol{l}_{\mathcal{C},3}$ and $J_{3,3}$ denote the third element of $\boldsymbol{l}_{\mathcal{C}}$ and the third row-third column element of $\mathbf{J}_1 \left(\boldsymbol{\eta}_{\mathbf{2}} \right)$ respectively. Finally, $\boldsymbol{w}_{\boldsymbol{p}}^{cam}$, $\boldsymbol{w}_{of}^{cam}$ and n_z^{cam} represent the gaussian noises of the camera sensor for the position, optical flow and range measurements.

The proposed sensor fusion structure (see Fig. 1.7) builds an estimated state vector $\hat{\boldsymbol{s}} = \left[\hat{\boldsymbol{n}}_{\mathbf{1}}^T \; \hat{\boldsymbol{v}}_{\mathbf{1}}^T \; \hat{\boldsymbol{b}}_{\boldsymbol{a}}^T \right]^T$ that involves the position $\hat{\boldsymbol{n}}_{\mathbf{1}} = [\hat{x} \; \hat{y} \; \hat{z}]^T$ expressed in $\boldsymbol{I}$ as well as the linear velocity $\hat{\boldsymbol{v}}_{\mathbf{1}} = [\hat{u} \; \hat{v} \; \hat{w}]^T$ and the accelerometer bias $\hat{\boldsymbol{b}}_{\boldsymbol{a}} = \left[\hat{b}_x \; \hat{b}_y \; \hat{b}_z \right]^T$ both expressed in $\boldsymbol{B}$. Recalling (1.18)-(1.24) and following [19], the proposed State

Estimation Module is summarized as:

$$\begin{aligned}
\hat{x}^{k+1} &= \hat{x}^{k,-} + k_{cam}^{x}\left(x^{cam,k} - \hat{x}^{k,-}\right)\\
\hat{y}^{k+1} &= \hat{y}^{k,-} + k_{cam}^{y}\left(y^{cam,k} - \hat{y}^{k,-}\right)\\
\hat{z}^{k+1} &= \hat{z}^{k,-} + k_{cam}^{z}\left(z^{cam,k} - \hat{z}^{k,-}\right) + k_{l}^{z}\left(z_{l}^{cam,k} - \hat{z}^{k,-}\right)\\
\hat{\boldsymbol{v}}_{\mathbf{1}}^{k+1} &= \hat{\boldsymbol{v}}_{\mathbf{1}}^{k,-} + \mathbf{K}_{cam}^{\boldsymbol{v_1}}\left(\boldsymbol{v}_{\mathbf{1}}^{cam,k} - \hat{\boldsymbol{v}}_{\mathbf{1}}^{k,-}\right)\\
\hat{\boldsymbol{b}}_{\boldsymbol{a}}^{k+1} &= \hat{\boldsymbol{b}}_{\boldsymbol{a}}^{k,-} - \mathbf{K}_{cam}^{\boldsymbol{b_a}}\left(\boldsymbol{v}_{\mathbf{1}}^{cam,k} - \hat{\boldsymbol{v}}_{\mathbf{1}}^{k,-}\right)
\end{aligned} \tag{1.27}$$

where

$$\begin{aligned}
\begin{bmatrix} x^{cam,k} \\ y^{cam,k} \\ z^{cam,k} \end{bmatrix} = \boldsymbol{\eta}_{\mathbf{1}}^{cam,k} &= \mathbf{R}_{\boldsymbol{IN}}\mathbf{R}^{IMU}\left(\mathbf{R}_{\mathcal{C}}^{T}\boldsymbol{p}_{\mathcal{C}}^{cam,k} - \boldsymbol{l}_{\mathcal{C}}\right)\\
z_{l}^{cam,k} &= -(J_{3,3}z_{\mathcal{C}}^{cam,k} - \boldsymbol{l}_{\mathcal{C},3})\\
\boldsymbol{v}_{\mathbf{1}}^{cam,k} &= z_{\mathcal{C}}^{cam,k}\mathbf{R}_{\mathcal{C}}^{T}\left(\boldsymbol{v}_{of}^{cam,k} - \mathbf{M}_{of}\mathbf{R}_{\mathcal{C}}\boldsymbol{\omega}_{\boldsymbol{B}}^{IMU}\right) - \boldsymbol{\omega}_{\boldsymbol{B}}^{IMU} \times \boldsymbol{l}_{\mathcal{C}}
\end{aligned} \tag{1.28}$$

and the a priori estimate $\hat{\boldsymbol{s}}^{k,-} = [\hat{\boldsymbol{\eta}}_{\mathbf{1}}^{k,-^T}, \hat{\boldsymbol{v}}_{\mathbf{1}}^{k,-^T}, \hat{\boldsymbol{b}}_{\boldsymbol{a}}^{k,-^T}]^T$ is calculated by:

$$\begin{aligned}
\hat{\boldsymbol{\eta}}_{\mathbf{1}}^{k,-} &= \hat{\boldsymbol{\eta}}_{\mathbf{1}}^{k} + \Delta t\,\mathbf{R}_{\boldsymbol{IN}}\mathbf{R}^{IMU,k}\hat{\boldsymbol{v}}_{\mathbf{1}}^{k}\\
\hat{\boldsymbol{v}}_{\mathbf{1}}^{k,-} &= \hat{\boldsymbol{v}}_{\mathbf{1}}^{k,-} + \Delta t\left(\boldsymbol{a}_{\boldsymbol{B},k}^{IMU} - \hat{\boldsymbol{b}}_{\boldsymbol{a}}^{k} + \mathbf{R}_{IMU}^{k}\boldsymbol{g}_{\boldsymbol{I}}\right)\\
\hat{\boldsymbol{b}}_{\boldsymbol{a}}^{k,-} &= \hat{\boldsymbol{b}}_{\boldsymbol{a}}^{k}
\end{aligned} \tag{1.29}$$

Finally, k_{cam}^{x}, k_{cam}^{y}, k_{cam}^{z} and k_{l}^{z} are positive gains that depend on the selected cut-off frequencies of the camera position and range measurements, and $\mathbf{K}_{cam}^{\boldsymbol{v_1}}$ and $\mathbf{K}_{cam}^{\boldsymbol{b_a}}$ are positive diagonal matrices that depend on the selected cut-off frequency and damping of the optical flow measurements. It should also be noted that based on standard gain tuning techniques for Complementary Filters [19], the overall stability of the estimation scheme is guaranteed under the following conditions:

$$\begin{aligned}
k_{cam}^{i} &< 1,\ i \in \{x, y\}\\
k_{cam}^{z} + k_{l}^{z} &< 1\\
\mathbf{K}_{cam}^{\boldsymbol{v_1}} &< \mathbf{I}_3\\
\mathbf{K}_{cam}^{\boldsymbol{b_a}} &< \Delta t\,\boldsymbol{\Omega_c}
\end{aligned} \tag{1.30}$$

where $\boldsymbol{\Omega_c}$ is a diagonal matrix that involves the selected cut-off frequencies of the optical flow measurements in all axes.

1.3.2.2 Deep Waters Operation

In deep waters, vision sensors may present reduced performance due to low visibility and poor lighting conditions. In that case, the standard AHRS-depth sensor

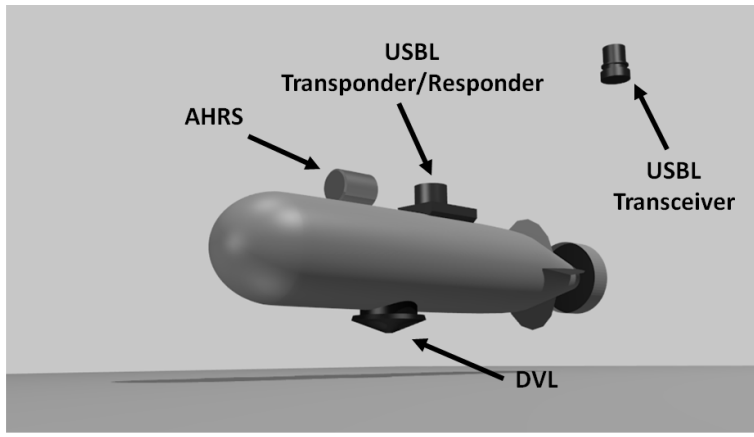

Figure 1.9: Sensor setup for deep waters operation.

suite is enriched with additional acoustic navigation sensors, such as a DVL and/or a USBL. The DVL sensor delivers measurements of the vehicle linear velocity with respect to the seabed. The principal operation of the sensor is based on the transmission of acoustic pings through the water and measurement of the reflections on the seabed [22] via a multi-beam echo-sounder. A doppler shift appears in the reflections which can be used to calculate the velocity of the underwater vehicle. The output measurements are given with respect to the sensor fixed coordinate system $\boldsymbol{S_{DVL}}$. Assuming that the distance between the DVL sensor and the body frame $\boldsymbol{B}$ is $\boldsymbol{l_{DVL}}$ and $\boldsymbol{R_{DVL}}$ is the is the rotation matrix from the body frame $\boldsymbol{B}$ to the DVL frame $\boldsymbol{S_{DVL}}$, the following measurement equation for the linear velocity stands:

$$\boldsymbol{v^{DVL}} = \boldsymbol{R_{DVL}}\,(\boldsymbol{v_1} + \boldsymbol{v_2} \times \boldsymbol{l_{DVL}}) + \boldsymbol{w_{v_{DVL}}} \tag{1.31}$$

where $\boldsymbol{w_{v_{DVL}}}$ is measurement noise due to a scale error produced by the uncertainty of the speed of sound within the water, which in turn is highly affected by the water salinity.

A USBL system consists of a transceiver, which is mounted on a fixed position (e.g under a ship) and a transponder or responder which is rigidly attached on the underwater vehicle, as shown in Fig. 1.9. The 3D position of the vehicle is calculated by the ranges and bearings measured by the transceiver. An acoustic pulse is transmitted by the transceiver and detected by the on–board transponder, which in turn replies with its own acoustic pulse. This latter is detected by the transceiver. The time duration from the initial transmission until the detected reply is converted into range. The bearings are measured by the transceiver, which contains an array of transducers (usually three or more).

For the sake of simplicity, we assume that the Inertial frame $\boldsymbol{I}$ coincides with the transceiver's frame. The USBL delivers position measurements $\boldsymbol{p^I{}_{RSP}}$ of the responder with reference frame $\boldsymbol{U_{RSP}}$ with respect to $\boldsymbol{I}$. Assuming that the distance between the responder and the body frame $\boldsymbol{B}$ is $\boldsymbol{l_{RSP}}$ and $\boldsymbol{R_{RSP}}$ is the is the rotation

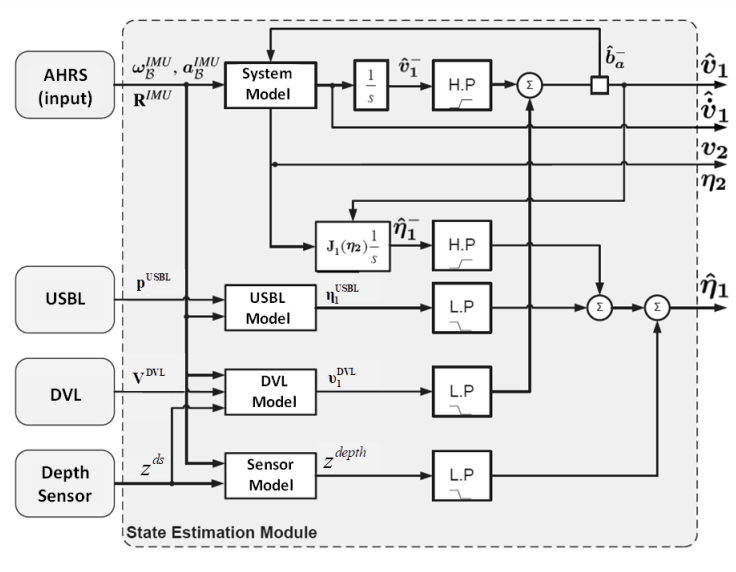

Figure 1.10: The proposed State Estimation Module for Deep Waters.

matrix from the body frame $\boldsymbol{B}$ to the responder frame $\boldsymbol{U_{RSP}}$, the following measurement equation for the position of the vehicle stands:

$$\boldsymbol{p^{USBL}} = \boldsymbol{R_{RSP}}\left(\boldsymbol{J}\left(\boldsymbol{n_2}\right)\boldsymbol{n_1} + \boldsymbol{l_{RSP}}\right) + \boldsymbol{w_{p_{USBL}}} \tag{1.32}$$

The depth sensor measurements are based on the difference between the current pressure and the atmospheric. Assuming that the depth sensor frame coincides with the body frame $\boldsymbol{B}$, the relation between the depth sensor measurements and the vertical position of the vehicle is straightforward:

$$z^{ds} = \frac{z}{J_{3,3}} + w_z^{ds} \tag{1.33}$$

where z^{ds} is the measured depth and $J_{3,3}$ denotes the third row-third column element of $\mathbf{J}_1\left(\boldsymbol{\eta_2}\right)$. Finally, w_z^{ds}, represents the gaussian noise of the depth sensor for the vertical position measurements. The state model, as well as the AHRS measurement model, are exactly the same as in 1.18 and 1.20 respectively.

The proposed sensor fusion structure (see Fig. 1.10) builds an estimated state vector $\hat{\boldsymbol{s}} = \left[\hat{\boldsymbol{n}}_{\boldsymbol{1}}^T\ \hat{\boldsymbol{v}}_{\boldsymbol{1}}^T\ \hat{\boldsymbol{b}}_{\boldsymbol{a}}^T\right]^T$ that involves the position $\hat{\boldsymbol{n}}_{\boldsymbol{1}} = [\hat{x}\ \hat{y}\ \hat{z}]^T$ expressed in $\boldsymbol{I}$, which in this case coincides with the transceiver's frame, as well as the linear velocity $\hat{\boldsymbol{v}}_{\boldsymbol{1}} = [\hat{u}\ \hat{v}\ \hat{w}]^T$ and the accelerometer bias $\hat{\boldsymbol{b}}_{\boldsymbol{a}} = \left[\hat{b}_x\ \hat{b}_y\ \hat{b}_z\right]^T$ both expressed in $\boldsymbol{B}$. Recalling (1.18)-(1.20) and following [19], the proposed State Estimation Module is

summarized as:

$$\begin{aligned}
\hat{x}^{k+1} &= \hat{x}^{k,-} + k^{x}_{USBL}\left(x^{USBL,k} - \hat{x}^{k,-}\right)\\
\hat{y}^{k+1} &= \hat{y}^{k,-} + k^{y}_{USBL}\left(y^{USBL,k} - \hat{y}^{k,-}\right)\\
\hat{z}^{k+1} &= \hat{z}^{k,-} + k^{z}_{USBL}\left(z^{USBL,k} - \hat{z}^{k,-}\right) + k^{z}_{depth}\left(z_l^{depth,k} - \hat{z}^{k,-}\right)\\
\hat{\boldsymbol{v}}_{\mathbf{1}}^{k+1} &= \hat{\boldsymbol{v}}_{\mathbf{1}}^{k,-} + \mathbf{K}^{\boldsymbol{v_1}}_{DVL}\left(\boldsymbol{v}_{\mathbf{1}}^{DVL,k} - \hat{\boldsymbol{v}}_{\mathbf{1}}^{k,-}\right)\\
\hat{\boldsymbol{b}}_{\boldsymbol{a}}^{k+1} &= \hat{\boldsymbol{b}}_{\boldsymbol{a}}^{k,-} - \mathbf{K}^{\boldsymbol{b_a}}_{DVL}\left(\boldsymbol{v}_{\mathbf{1}}^{DVL,k} - \hat{\boldsymbol{v}}_{\mathbf{1}}^{k,-}\right)
\end{aligned} \tag{1.34}$$

where

$$\begin{aligned}
\begin{bmatrix} x^{USBL,k} \\ y^{USBL,k} \\ z^{USBL,k} \end{bmatrix} &= J(\boldsymbol{\eta_2})\left(\boldsymbol{R}^{\boldsymbol{T}}_{RSP}\boldsymbol{p}^{USBL,k} - \boldsymbol{l}_{RSP}\right)\\
z_l^{depth,k} &= -J_{3,3}z^{ds,k}\\
\boldsymbol{v}_{\mathbf{1}}^{DVL,k} &= \boldsymbol{R}^{\boldsymbol{T}}_{DVL}\boldsymbol{V}^{DVL,k} - \boldsymbol{l}_{DVL}
\end{aligned} \tag{1.35}$$

and the a priori estimate $\hat{\boldsymbol{s}}^{k,-} = [\hat{\boldsymbol{\eta}}_{\mathbf{1}}^{k,-^T}, \hat{\boldsymbol{v}}_{\mathbf{1}}^{k,-^T}, \hat{\boldsymbol{b}}_{\boldsymbol{a}}^{k,-^T}]^T$ is calculated by:

$$\begin{aligned}
\hat{\boldsymbol{\eta}}_{\mathbf{1}}^{k,-} &= \hat{\boldsymbol{\eta}}_{\mathbf{1}}^{k} + \Delta t\mathbf{R}^{IMU,k}\hat{\boldsymbol{v}}_{\mathbf{1}}^{k}\\
\hat{\boldsymbol{v}}_{\mathbf{1}}^{k,-} &= \hat{\boldsymbol{v}}_{\mathbf{1}}^{k,-} + \Delta t\left(\boldsymbol{a}_{\boldsymbol{B},k}^{IMU} - \hat{\boldsymbol{b}}_{\boldsymbol{a}}^{k} + \mathbf{R}^{k}_{IMU}\boldsymbol{g_1}\right)\\
\hat{\boldsymbol{b}}_{\boldsymbol{a}}^{k,-} &= \hat{\boldsymbol{b}}_{\boldsymbol{a}}^{k}
\end{aligned} \tag{1.36}$$

Finally, k^{x}_{USBL}, k^{y}_{USBL}, k^{z}_{USBL} and k^{z}_{depth} are positive gains that depend on the selected cut-off frequencies of the USBL and depth sensor measurements, and $\mathbf{K}^{\boldsymbol{v_1}}_{DVL}$ and $\mathbf{K}^{\boldsymbol{b_a}}_{DVL}$ are positive diagonal matrices that depend on the selected cut-off frequency and damping of the DVL measurements. It should also be noted that based on standard gain tuning techniques for Complementary Filters [19], the overall stability of the estimation scheme is guaranteed under the following conditions:

$$\begin{aligned}
k^{i}_{USBL} &< 1,\ i \in \{x,y\}\\
k^{z}_{USBL} + k^{z}_{l} &< 1\\
\mathbf{K}^{\boldsymbol{v_1}}_{DVL} &< \mathbf{I}_3\\
\mathbf{K}^{\boldsymbol{b_a}}_{DVL} &< \Delta t\boldsymbol{\Omega_{dvl}}
\end{aligned} \tag{1.37}$$

where $\boldsymbol{\Omega_{dvl}}$ is a diagonal matrix that involves the selected cut-off frequencies of the DVL measurements in all axes.

1.4 Results

In this section we present experimental results related to the state estimation and system identification of a small underwater vehicle operating in shallow waters. More

specific, the experiments were carried out inside the *NTUA, Control Systems Lab* test tank, with dimensions $5m \times 3m \times 1.5m$. The bottom of the tank is covered by a custom-made poster with various visual features and markers. The vehicle used in this work is a 4 DoFs Seabotix LBV [17], actuated in Surge, Sway, Heave and Yaw via a 4 thruster set configuration. The vehicle is equipped with a down-looking Sony PlayStation Eye camera, with 640×480 pixels at 30 frames per second (fps) enclosed in a waterproof housing. An underwater laser pointer projecting a green dot at the bottom of the test tank is rigidly attached on the vehicle with its axes aligned to the down-looking camera axis. The vehicle is also equipped with an $SBG\,IG-500A$ AHRS, delivering temperature-compensated 3D acceleration, angular velocity and orientation measurements at $100Hz$. Finally, the marker localization system is based on the $ArUco$ library [20] and the software implementation of the proposed identification scheme as well as of the motion control schemes was conducted in C++ and Python under the Robot Operating System (ROS) [23].

1.4.1 State Estimation Results

Notice that the $3D$ acceleration, angular velocity and orientation measurements are acquired by the on-board AHRS. Thus, the goal of the State Estimation Module is to deliver the 3D position and linear velocities of the vehicle. Based on Complementary Filters technique, the selection of the appropriate cut-off frequencies is based on the reliability of both sensors, system model and the camera algorithms in certain bands of frequency. In our case, the accelerometer sensor suffers from bias below $4Hz$, while optical flow algorithm gives reliable measurements up to $5Hz$ for x-y axes and up to $3Hz$ frequency for z-axis. Furthermore, due to unreliable data of optical flow in z-axis against x-y axes we select $\zeta_z = 0.5$ and $\zeta_{x,y} = 3$, thus $\mathbf{K}_{cam}^{\boldsymbol{\nu_1}} = diag\{0.3,\ 0.3,\ 0.06\}$ and $\mathbf{K}_{cam}^{\boldsymbol{b_a}} = diag\{0.2,\ 0.2,\ 0.2\}$. Regarding the F and R axes position filters, the marker based localization measurements (Aruco) were proven to exhibit unsatisfactory behavior over $6Hz$, thus we selected $k_{cam}^{x} = 0.09$ and $k_{cam}^{y} = 0.09$. Finally, the depth measurements based on laser algorithm proved of good quality in a low bandwidth up to $2Hz$, while the same data captured by the Aruco algorithm were more reliable in higher frequencies ($4Hz$), thus we selected $k_{cam}^{z} = 0.05$ and $k_{l}^{z} = 0.003$. It should be noted here that the sensors and the appropriate camera algorithms run in different time frames. Thus, the aforementioned gains were selected accordingly.

Using the aforementioned gains, in Fig. 1.11 the estimated horizontal position of the vehicle is depicted (blue line) along with the position measurement provided by the marker localization algorithm (red line). It is worth noting that even when there is no absolute localization measurement (no marker inside the camera field of view), the Complementary Filter algorithm that is adopted in the State Estimation Module, is able to provide valid estimations of the position vector $\boldsymbol{\eta_1}$ without significant drift, improving in this way the robustness of the state estimation. The estimated longitudinal and lateral velocities are depicted (blue line) in Fig. 1.12 along with the corresponding velocity measurements obtained by the optical flow technique (red line). The estimated depth and vertical velocity of the vehicle are

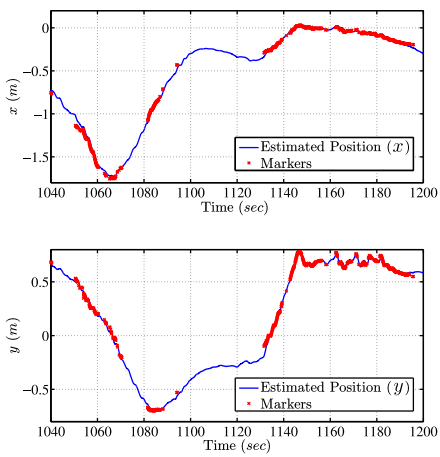

Figure 1.11: The estimated horizontal position of the vehicle.

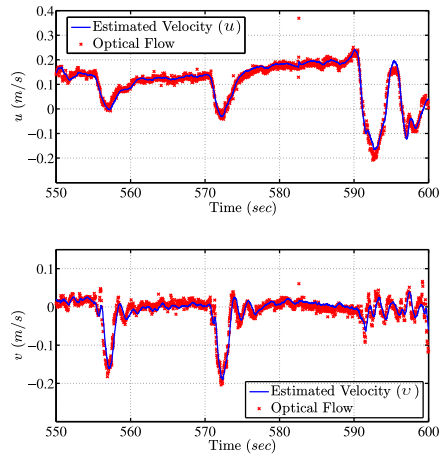

Figure 1.12: The estimated longitudinal and lateral velocities of the vehicle.

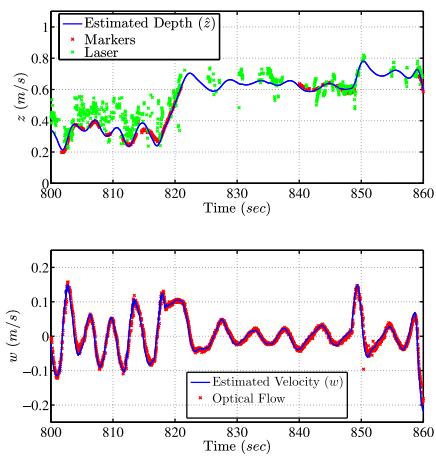

Figure 1.13: The estimated depth of the vehicle.

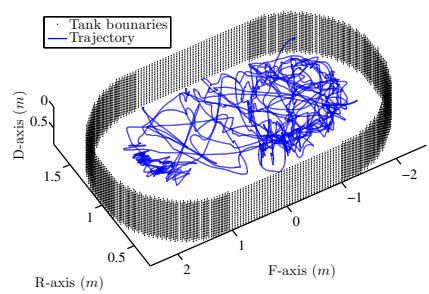

Figure 1.14: The trajectory of the vehicle during the identification procedure.

depicted in Fig. 1.13 along with the corresponding measurements acquired by the laser-based technique, the marker localization framework and the optical flow technique. In the same figure the estimated vertical velocity of the vehicle is provided along with the velocity measurements acquired by the optical flow technique.

1.4.2 On-line Parameter Identification Results

The evolution of the parameters related to the Surge, Sway, Heave and Yaw DoFs during the corresponding excitation modes are depicted in Fig. 1.15 and Fig. 1.16. The ultimate convergence of the parameters during *modeTotal* is shown in Fig. 1.17 and Fig. 1.18. Moreover, the trace of the corresponding covariance matrices P_{surge}, P_{sway}, P_{heave} and P_{yaw} is depicted in Fig. 1.19, from which we may observe that the trace for each DoF, reduces gradually and converges ultimately to a small positive value. It is worth noting that no prior knowledge of the parameter vector was employed since the initial values for all parameters were set to zero. Nevertheless, the evolution of the parameter estimates, shows that all parameters converged to a steady state value after a relatively short period of time. The estimated parameter set is shown in Table 1.1.

As it can be observed from the experimental results, the total duration of the procedure for the demonstrated experiment was approximately 330 s. The duration varies, since certain factors affect the final result. More specifically, apart from the covariance matrix trace convergence, the characteristics of the input signals (frequencies, amplitudes) may affect the total duration of the identification procedure. In our case, the last were chosen in order to produce full iterations in every trajectory set. The effect of the tether and the initial configuration may also slightly affect the final result. However, since the model parameters are not time varying and the excitation sequence is the same in every experiment: Yaw, Surge, Sway Heave, Total, the parameters converge to close values each time. Additionally, the random inputs exerted by the Excitation Module, secure that the regression matrix Y is always full rank, thus we do not anticipate significant deviations on the results of each identification procedure.

When a mode is completed, as indicated by the appropriate metric, the algorithm pauses the further update of the parameters related to that specific mode. But, when modeTotal is engaged, the estimation resumes for all the parameters, until the final convergence. As it can be seen by observing Fig.1.15 - 1.18, the final values estimated by modeTotal are not too far from the values calculated by the individual modes.

The terminating values for each mode are: $P^{\star}_{yaw} = 0.08$, $P^{\star}_{surge} = 0.25$, $P^{\star}_{sway} = 0.25$, $P^{\star}_{heave} = 0.5$, $P^{\star}_{total} = 0.3$. As it can be observed $P^{\star}_{yaw}$ was assigned with the smallest value since the angle and angular velocity are directly obtained from the IMU which has very small measurement noise. On the contrary, the motion along Surge and Sway are estimated via the Complementary Filter thus, the terminating values are higher. The same stands for the motion estimation along Heave axis, where additionally the measurements of the less reliable sensors (Depth Sensor and Laser) are employed, hence the terminating value is larger. The value of $P^{\star}_{total}$ was selected to be approximately 30% of the sum of the individual modes.

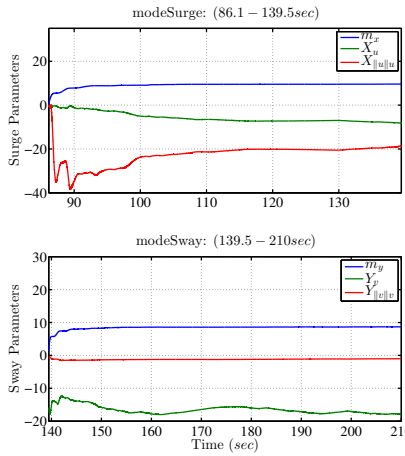

Figure 1.15: The evolution of the parameter estimates for the Surge and Sway DoFs, during the corresponding excitation modes.

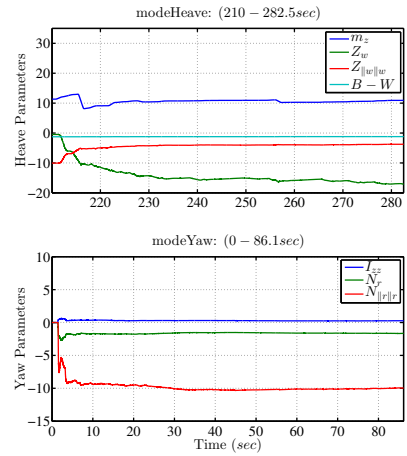

Figure 1.16: The evolution of the parameter estimates for the Heave and Yaw DoFs, during the corresponding excitation modes.

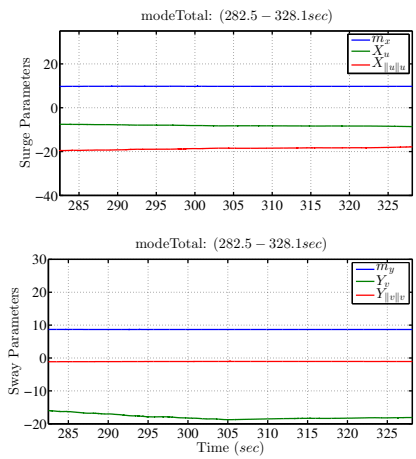

Figure 1.17: The evolution of the parameter estimates for the Surge and Sway DoFs, during *modeTotal*.

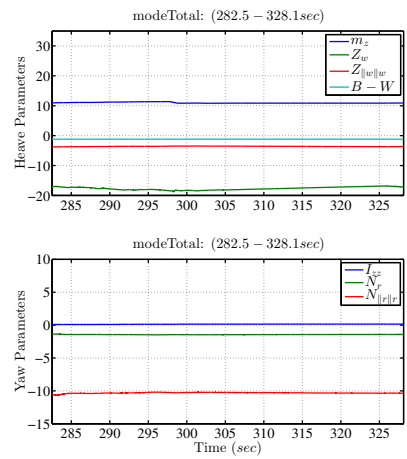

Figure 1.18: The evolution of the parameter estimates for the Heave and Yaw DoFs, during *modeTotal*

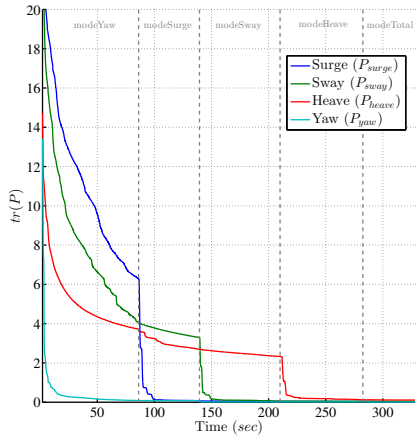

Figure 1.19: The evolution of the trace of the covariance matrices for the Surge, Sway, Heave and Yaw DoFs.

Table 1.1: The identified parameter set.

m_x	m_y	m_z	I_z
9.7532	8.6636	10.898	0.1589
X_u	Y_v	Z_w	N_r
−8.6040	−18.1106	−17.1828	−1.4146
$X_{\|u\|u}$	$Y_{\|v\|v}$	$Z_{\|w\|w}$	$N_{\|r\|r}$
−17.8534	−1.0594	−3.6482	−10.3483
		$W-B$	
		−1.1881	

References

[1] Fossen T. Guidance and Control of Ocean Vehicles. Wiley, New York. 1994;.

[2] Bishop R, Parkinson AG. ON THE PLANAR MOTION MECHANISM USED IN SHIP MODEL TESTING. Phil Trans Roy Soc London Ser AMath Phys Sci. 1970;266(1171):35–61.

[3] Avila JPJ, Adamowski JC. Experimental evaluation of the hydrodynamic coefficients of a ROV through Morison's equation. Ocean Engineering. 2011;38(17-18):2162–2170.

[4] Evans J, Nahon M. Dynamics modeling and performance evaluation of an autonomous underwater vehicle. Ocean Engineering. 2004;31(14-15):1835–1858.

[5] Sahin I, Crane JW, Watson KP. Application of a panel method to hydrodynamics of underwater vehicles. Ocean Engineering. 1997;24(6):501–512.

[6] Smallwood D, Whitcomb L. Adaptive identification of dynamically positioned underwater robotic vehicles. IEEE Transcactions on Control Systems Technology. 2003;p. 505–515.

[7] McFarland CJ, Whitcomb LL. Comparative experimental evaluation of a new adaptive identifier for underwater vehicles. In: Proceedings - IEEE International Conference on Robotics and Automation; 2013. p. 4614–4620.

[8] van de Ven P, Johansen T, Sorensen A, et al. Neural network augmented identification of underwater vehicle models. Control Engineering Practice 15. 2007;.

[9] Ishii K, Fujii T, Ura T. An On-line Adaptation Method in a Neural Network Based Control System for AUV's. IEEE Journal of Oceanic Engineering. 1995;20(3):221–228.

[10] Eng YH, Teo KM, Chitre M, et al. Online System Identification of an Autonomous Underwater Vehicle Via In-Field Experiments. IEEE Journal of Oceanic Engineering. 2016 Jan;41(1):5–17.

[11] Karras GC, Bechlioulis CP, Leonetti M, et al. On-line identification of autonomous underwater vehicles through global derivative-free optimization. In: IEEE International Conference on Intelligent Robots and Systems; 2013. p. 3859–3864.

[12] Julier S, Uhlmann J. A new extension of the kalman filter to nonlinear systems. Procof the Int Symp Aerospace/Defense Sensing, Simul and Controls. 1997;.

[13] Cutipa Luque JC, Donha DC. AUV identification and robust control. In: IFAC Proceedings Volumes (IFAC-PapersOnline). vol. 18; 2011. p. 14735–14741.

[14] der Merwe RV, Wan E. The square-root unscented Kalman filter for state and parameter-estimation. IEEE International Conference on Acoustics, Speech, and Signal Processing. 2001;p. 3461–3464.

[15] VanDyke M, Schwartz J, Hall C. Unscented Kalman Filtering for Spacecraft Attitude State and Parameter Estimation. Advances in the Astronautical Sciences. 2004;p. 217–228.

[16] Karras GC, Loizou SG, Kyriakopoulos KJ. Towards semi-autonomous operation of under-actuated underwater vehicles: sensor fusion, on-line identification and visual servo control. Autonomous Robots. 2011;p. 67–86.

[17] Seabotix LBV150;. Available from: http://www.teledynemarine.com/lbv150-4/?BrandID=19.

[18] Ioannou P, Sun J. Robust Adaptive Control. New Jersey, U.S.A.: Prentice Hall; 1996.

[19] Marantos P, Koveos Y, Kyriakopoulos KJ. UAV State Estimation Using Adaptive Complementary Filters. Control Systems Technology, IEEE Transactions on. 2016 Jul;24(4):1214–1226.

[20] Garrido-Jurado S, noz Salinas RM, Madrid-Cuevas FJ, et al. Automatic generation and detection of highly reliable fiducial markers under occlusion. Pattern Recognition. 2014;47(6):2280 – 2292.

[21] Karras GC, Kyriakopoulos KJ, Karavas GK. Towards cooperation of underwater vehicles: A Leader-Follower scheme using vision-based implicit communications. In: Intelligent Robots and Systems (IROS), 2015 IEEE/RSJ International Conference on; 2015. p. 4852–4857.

[22] Instruments R. Navigator ADCP/DVL Technical Manual;.

[23] Robot Operating System;. Available from: http://www.ros.org/.